FULL LENGTH PAPER

LATERAL ADAPTIVE CONTROL OF PARAFOIL-PAYLOAD SYSTEM

Prateek Sazawal
Project Associate
Department of Aerospace Engineering
Indian Institute of Technology Kanpur
Kanpur-208 016, India
Email : prateeksazawal@ gmail.com

A.K. Ghosh
Professor
Department of Aerospace Engineering
Indian Institute of Technology Kanpur
Kanpur-208 016, India
Email : akg@iitk.ac.in

Abstract

The motion of a parafoil is characterized by nonlinear dependence of aerodynamic loads on angle of attack. Nonlinear dynamics and non-rigidity of parafoil-payload system causes difficulty in estimating aerodynamic coefficients of the parafoil with respect to angular rates. The present paper addresses the problem of lateral control of a generic 9 degree of freedom parafoil-payload system under small perturbations. A Lyapunov based dynamic adaptive controller is proposed in order to control such a system with known static coefficients and unknown dynamic coefficients. It is demonstrated numerically that the proposed controller is capable of controlling the system without estimating dynamic coefficients (theoretically or experimentally).

Nomenclature

a	= Unknown parameter vector
â	= Estimated parameter vector
AR	= Parafoil aspect ratio
b, c, t	= Parafoil span, chord length and thickness
C_{Db}	= Payload drag coefficient
C_L, C_D	= Lift and drag coefficients of parafoil
C_l, C_m, C_n	= Parafoil aerodynamic moment coefficients
C_x, C_y, C_z	= Parafoil aerodynamic load coefficients
$e_{\delta a}$	= Error in asymmetric deflection angle
$\mathbf{F}$	= Force vector
$\mathbf{F}_o$	= Force exerted at the joint point
$\mathbf{I}$	= Identity matrix
$\boldsymbol{I}$	= Moment of inertia matrix
$\boldsymbol{I}_F$	= Apparent moment of inertia matrix
k_o, c_o	= Stiffness and damping at the joint point
g	= Acceleration due to gravity
m	= Mass
$\mathbf{M}$	= Moment vector
$\boldsymbol{M}_F$	= Apparent mass matrix of parafoil
$\boldsymbol{M}_{in}$	= Mass matrix of air inside parafoil
$\boldsymbol{M}_p$	= Parafoil canopy mass matrix
$\mathbf{M}_o$	= Moment exerted at the joint point
p, q, r	= Roll, pitch and yaw rate
R_{op}, R_{ob}	= Parafoil and payload link lengths measured from the joint point
S	= Planform area
$\boldsymbol{S}$	= Reference frame fixed to a body
$\mathbf{T}$	= Transformation matrix
u, v, w	= Component of velocity along the three axes
u_{act}	= Actuator input
U	= Speed of a body
$\mathbf{v}$	= Velocity vector
V	= Lyapunov function
x, y, z	= Position in Cartesian coordinate system
$\mathbf{x}$	= Position vector
$\mathbf{X}$	= System state vector
α	= Angle of attack
β	= Sideslip angle
δ_a	= Asymmetric deflection angle of parafoil
δ_s	= Symmetric deflection angle of parafoil
Θ	= Attitude vector
μ	= Parafoil rigging angle
ρ	= Density of air at sea level
ϕ, θ, ψ	= Roll, pitch and yaw angle
ω	= Angular velocity
$\Re^{mxn}$	= Real vector space of dimension m x n

Paper Code : V67 N2/829-2015. Manuscript received on 03 Jul 2013. Reviewed, revised and accepted as a Full Length Contributed Paper on 04 Mar 2015

Subscript

b	= Referred to payload
p	= Referred to parafoil
i	= Referred to either payload or parafoil ($i = b, p$)
A	= Referred to aerodynamic
G	= Referred to gravitational
trim	= Referred to trim condition
o	= Referred to joint point
p, q, r	= Angular rate stability derivatives
α_p, β_p	= Wind direction stability derivatives
δ_a, δ_s	= Control surface derivatives

Superscripts

x	= Cross product matrix operator
T	= Transpose operator on a matrix
-1	= Inverse operator on a square matrix

Introduction

Guided ram air parafoils are long known for their applications in cargo delivery and recovery systems. They are cheap and easy to deploy due to compact size and light weight. Parafoil is an inflated non-rigid wing made of fabric. The airfoil shape provides the lift along with drag, unlike parachute where drag is the dominant component of aerodynamic force. Parafoils have controllable flexible flaps near the trailing edge which act as elevons as shown in Fig.1. The development of parafoil applications goes back to 1964 by Domina Jalbert. The first powered parafoil system called Aeroflyer was built by John D. Nicolaides [1]. Despite these inventions, a significant literature in control techniques of the parafoil-payload system is reported only in the last decade. One of the major problems encountered in the history of parafoil systems is the payload oscillation, since it is influenced by gusts.

Recent advancements in guided parafoil systems include spacecraft and unmanned air vehicle recovery because they provide precise and soft landing of the payload. In 1995, the Guided Parafoil Airborne Delivery System (GPADS) program demonstrated the stabilization and touchdown precision of parafoil systems having a span of 150 ft. with a number of military payloads at high altitudes [2].

The trailing edge flaps may have angular deflections in the same direction or opposite direction similar to elevon deflection in aircrafts. There are two types of control actuation techniques defined for a parafoil system, namely symmetrical and asymmetrical brake deflections. The symmetric brake deflection is responsible for change in glide slope of the parafoil system. An important aspect of the parafoil-payload system control was made by Slegers and Costello [4] in 2003 by pointing out the two counter modes of lateral control, namely roll steering and skid steering. Roll steering corresponds to a dominant rolling motion of the system, due to dominant differential lift force, when an asymmetric brake deflection is applied. On the other hand, if there is a dominant yaw motion, due to dominant differential drag force, for the same asymmetric deflection, the mode is called skid steering. The asymmetric brake deflection causes banking of the system in opposite directions depending on which of the two modes is active. Slegers and Costello [4] also found that change in the canopy curvature and magnitude of the asymmetric brake deflection causes a transition between the two modes.

The parafoil payload system has aerodynamic coefficients which are highly nonlinear functions of angle of attack and brake deflections [5]. Another important aerodynamic design aspect of parafoil systems is the angle between parafoil linkage and parafoil roll axis, called the rigging angle. Prakash and Ananthkrishnan [5] analysed the gliding and turning flights of a parafoil-payload system using 9 degree of freedom dynamic model for different rigging angles and symmetric and asymmetric brake deflections.

A model predictive control strategy for parafoil-payload system was presented by Slegers and Costello [7] using a 6 degree of freedom reduced state linear dynamic model. Gorman and Slegers [6] also showed that a 6 degree of freedom simulation model is inadequate to produce all significant motion of the system.

Longitudinal control of parafoil-payload system is difficult to achieve and has a limited account in the literature. A longitudinal control technique of glide slope by change in incidence angle is reported by Slegers et al. [8]. For this purpose, the authors used rigging changes and an additional servoactuator.

The determination of parafoil aerodynamic coefficients is a difficult task. Due to non-rigid structure of the parafoil, mounting conventional motion sensors on the canopy is troublesome. However, measurement of static aerodynamic coefficients in a wind tunnel is relatively easier. The objective of the present work is to control the parafoil-payload system for unknown parafoil dynamic derivatives where the static derivatives are known. A

Lyapunov based dynamic adaptive controller for the parafoil-payload system is proposed which can handle lateral disturbances in the system. The present dynamic adaptive control law guarantees global asymptotic stability of the system, similar to the control law used by Slotine and Li [10] for robot manipulators. A 9 degree of freedom model of the system is considered for this purpose. Because of the complexity involved in achieving the longitudinal control of parafoil-payload system with the help of symmetric brake deflection, the asymmetric brake deflection is taken as the only control input with symmetric brake deflection being constant. For the analysis, the system (canopy and links) is assumed to be rigid and completely inflated at all times.

Parafoil-Payload System

Figure 1 shows an inflated parafoil-payload system at an angle of attack. Points P and B are respectively the centers of gravity of the parafoil and the payload. The parafoil is connected to the payload through the links OP and OB meeting at a common joint point O. S_p, S_b and S_o represents parafoil fixed, payload fixed and joint point fixed frames respectively. The [X_i, Y_i, Z_i] refers to the orthogonal axes of the frame S_i. The joint point fixed frame is chosen in such a way that two of its axes (X_o and Y_o) lie in horizontal plane and one axis (Z_o) is along the direction of gravity.

The three defined frames are mutually inclined to each other. The orientation of the parafoil fixed frame and payload fixed frame with respect to the joint point fixed frame can be represented using Euler 3-2-1 rotation sequence. Hence, quantities expressed in frame S_o can be transformed into payload or parafoil fixed frame coordinates as follows,

$$\begin{Bmatrix} x_i \\ y_i \\ z_i \end{Bmatrix} = \mathrm{T}_i \begin{Bmatrix} x_o \\ y_o \\ z_o \end{Bmatrix} \tag{1}$$

where, $\mathbf{T}_i$ is the transformation matrix for a body having an orientation of (ψ_i (3), θ_i (2), ϕ_i (3)) with respect to the joint point fixed frame (or earth fixed frame). It can be observed from Fig.1 that the system has 9 degrees of freedom defined independently by (x_o, y_o, z_o, ϕ_p, θ_p, ψ_p, ϕ_b, θ_b, ψ_b).

Parafoil-Payload Dynamics

The dynamics of the parafoil-payload system can be modelled by resolving the system into two subsystems, linked at the joint point. The load transfer between the parafoil and the payload takes place through the joint point O. The kinetic equations of the payload subsystem is given by,

$$m_b \left(\mathbf{T}_b \dot{\mathrm{v}}_o - [\mathrm{r}^{\times}_{ob}]\, \dot{\omega}_b + [\omega^{\times}_b]^2\, \mathbf{r}_{ob} \right) = \mathbf{F}_{bA} + \mathbf{F}_{bG} - \mathbf{T}_b\, \mathbf{F}_o \tag{2}$$

$$\boldsymbol{I}_b\, \dot{\omega}_b + [\omega^{\times}_b]\, \boldsymbol{I}_b\, \omega_b = \mathbf{T}_b\, \mathbf{M}_o + [\mathbf{r}^{\times}_{ob}]\, \mathbf{T}_b\, \mathbf{F}_o \tag{3}$$

where, $\mathbf{F}_o$ and $\mathbf{M}_o$ are the force and moment respectively, exerted on the payload by the joint point. Note that the joint forces and moments are expressed in joint point fixed frame, S_o. The apparent mass and moment of inertia plays a major role in the dynamics of the parafoil. Lissaman and Brown [9] provided the apparent mass and moment of inertia matrix for the inflated parafoil dynamics. The translational and rotational dynamic equations of motion of the parafoil subsystem [9] can be written as,

$$\begin{aligned} &(\boldsymbol{M}_p + \boldsymbol{M}_a)\, \mathbf{T}_p\, \dot{\mathbf{v}}_o - \boldsymbol{M}_p\, [\omega^{\times}_p]\, \mathbf{T}_p\, \mathbf{v}_o + [\omega^{\times}_p]\, \boldsymbol{M}_a\, \boldsymbol{T}_p\, \mathbf{v}_o \\ &- (\boldsymbol{M}_p + \boldsymbol{M}_a)\, [\mathbf{r}^{\times}_{op}]\, \dot{\omega}_p + [\omega^{\times}_p]\, (\boldsymbol{M}_p + \boldsymbol{M}_a)\, [\omega^{\times}_p]\, \mathbf{r}_{op} \\ &= \mathbf{F}_{pA} + \mathbf{F}_{pG} + \mathbf{T}_p\, \mathbf{F}_o \end{aligned} \tag{4}$$

$$\begin{aligned} &(\boldsymbol{I}_p + \boldsymbol{I}_F)\, \dot{\omega}_p + [\omega^{\times}_p]\, (\boldsymbol{I}_p + \boldsymbol{I}_F)\, \omega_p \\ &= \mathbf{M}_{pA} - \mathbf{T}_p\, \mathbf{M}_o - [\mathbf{r}^{\times}_{op}]\, \mathbf{T}_p\, \mathbf{F}_o \end{aligned} \tag{5}$$

where, $\boldsymbol{M}_a$ is the net included air mass and the apparent mass matrix of the parafoil. Therefore,

$$\boldsymbol{M}_a = \boldsymbol{M}_{in} + \boldsymbol{M}_F \tag{6}$$

The position vectors of point P and B in joint-point fixed frame are denoted by $\mathbf{r}_{op}$ and $\mathbf{r}_{ob}$ respectively, such that,

$$\begin{aligned} \mathbf{r}_{op} &= \{ -R_{op} \sin\mu\, ,\, 0,\, -R_{op} \cos\mu \}^T \\ \mathbf{r}_{ob} &= \{0,\, 0,\, R_{ob}\}^T \end{aligned} \tag{7}$$

Equations (2)-(5) can be easily grouped together in the form of a matrix equation,

$$\begin{bmatrix} -m_b[r_{ob}^{\times}] & 0\in\Re^{3\times3} & m_b T_b & T_b \\ 0\in\Re^{3\times3} & -(M_p+M_a)[r_{op}^{\times}] & (M_p+M_a)T_p & -T_p \\ I_b & 0\in\Re^{3\times3} & 0\in\Re^{3\times3} & -[r_{ob}^{\times}]T_b \\ 0\in\Re^{3\times3} & I_p+I_F & 0\in\Re^{3\times3} & [r_{op}^{\times}]T_p \end{bmatrix} \begin{Bmatrix} \dot{\omega}_b \\ \dot{\omega}_p \\ \dot{v}_o \\ F_o \end{Bmatrix} = \begin{Bmatrix} b_1 \\ b_2 \\ b_3 \\ b_4 \end{Bmatrix} \tag{8}$$

where,

$$\mathbf{b}_1 = \mathbf{F}_{bA} + \mathbf{F}_{bG} - m_b[\omega_b^{\times}]^2 \mathbf{r}_{ob} \tag{9}$$

$$\mathbf{b}_2 = \mathbf{F}_{pA} + \mathbf{F}_{pG} - [\omega_p^{\times}](\boldsymbol{M}_p + \boldsymbol{M}_a)[\omega_p^{\times}]\mathbf{r}_{op} + \boldsymbol{M}_p[\omega_p^{\times}]\mathbf{T}_p\mathbf{v}_o - [\omega_p^{\times}]\boldsymbol{M}_a\mathbf{T}_p\mathbf{v}_o \tag{10}$$

$$\mathbf{b}_3 = -[\omega_b^{\times}]\boldsymbol{I}_b\omega_b + \mathbf{T}_b\mathbf{M}_o \tag{11}$$

$$\mathbf{b}_4 = \mathbf{M}_{pA} - [\omega_p^{\times}](\boldsymbol{I}_p + I_F)\omega_p - \mathbf{T}_p\mathbf{M}_o \tag{12}$$

Equation (8) is the complete kinetic equation of motion of the 9 degree of freedom parafoil-payload system. It is important to note that the joint point force, $\mathbf{F}_o$ is not a state variable of the system. It is only an intermediate variable which exhibits the relation between dynamics of the payload subsystem and parafoil subsystem.

The links are free to rotate about the joint point, therefore no moment transfer is expected at point O. However in practice, the twisting of the links restricts the yawing motion of the payload with respect to parafoil. Therefore, it is assumed that moment transfer occurs only in the yaw direction and hence modelled in accordance to the spring-damper system [4]. It follows that,

$$\mathbf{T}_b\mathbf{M}_o = \begin{Bmatrix} 0 \\ 0 \\ k_o(\tilde{\psi}_p - \tilde{\psi}_b) + c_o(\dot{\tilde{\psi}}_p - \dot{\tilde{\psi}}_b) \end{Bmatrix} \tag{13}$$

where, $\tilde{\psi}_i$ and $\dot{\tilde{\psi}}_i$ are given by,

$$\tilde{\psi}_i = \tan^{-1}\frac{\sin\phi_i\sin\theta_i\cos\psi_i - \cos\phi_i\sin\psi_i}{\cos\theta_i\cos\psi_i} \tag{14}$$

$$\dot{\tilde{\psi}}_i = -\cos\tilde{\psi}_i\tan\tilde{\theta}_i\, p_i + \sin\tilde{\psi}_i\tan\tilde{\theta}_i\, q_i + r_i \tag{15}$$

$$\tilde{\theta}_i = \tan^{-1}\frac{(\cos\phi_i\sin\theta_i\cos\psi_i + \sin\phi_i\sin\psi_i)\cos\tilde{\psi}_i}{\cos\theta_i\cos\psi_i} \tag{16}$$

The kinematic equation of motion of the parafoil-payload system can be written as,

$$\dot{\mathbf{x}}_o = \begin{Bmatrix} u_o \\ v_o \\ w_o \end{Bmatrix} = \mathbf{v}_o \tag{17}$$

$$\dot{\Theta}_i = \begin{bmatrix} 1 & \sin\phi_i\tan\theta_i & \cos\phi_i\tan\theta_i \\ 0 & \cos\phi_i & -\sin\phi_i \\ 0 & \sin\phi_i/\cos\theta_i & \cos\phi_i/\cos\theta_i \end{bmatrix} \begin{Bmatrix} p_i \\ q_i \\ r_i \end{Bmatrix} = \mathbf{C}_i\omega_i \tag{18}$$

where,

$\mathbf{x}_o = \{x_o, y_o, z_o\}^T$, $\Theta_b = \{\phi_b, \theta_b, \psi_b\}^T$ $\Theta_p = \{\phi_p, \theta_p, \psi_p\}^T$ and are the position vector, payload attitude and parafoil attitude respectively. The 9 dynamic equations of motion given by Eq.(8) along with 9 kinematic equation of motion given by Eqs.(17) and (18) constitute the equation of motion of the parafoil-payload system. The kinematic relationship between payload/parafoil velocity and joint point velocity can be found using the transformation matrix in Eq.(1). It follows that,

$$\mathbf{v}_i = \mathbf{T}_i\mathbf{v}_o + [\omega_i^{\times}]\mathbf{r}_{oi} \tag{19}$$

The angle of attack and angle of sideslip of the parafoil are evaluated using the following equations,

$$\alpha_p = \tan^{-1}(w_p/u_p) \tag{20}$$

$$\beta_p = \sin^{-1}(v_p / U_p) \tag{21}$$

Aerodynamic Modelling

The aerodynamic drag force acting on the payload can be written as,

$$\mathbf{F}_{bA} = -\frac{1}{2}\rho\, U_b\, S_b\, C_{Db}\, \mathbf{v}_b \tag{22}$$

The center of pressure of the payload is taken at its center of mass. Also, it is assumed in the current study that the payload is bluff body. Hence, the drag is the only dominant aerodynamic force acting on the payload. The aerodynamic forces and moments acting on the parafoil is given by,

$$\mathbf{F}_{pA} = \frac{1}{2}\rho\, U_p^2\, S_p \begin{Bmatrix} C_x \\ C_y \\ C_z \end{Bmatrix} \tag{23}$$

$$\mathbf{M}_{pA} = \frac{1}{2}\rho\, U_p^2\, S_p \begin{Bmatrix} b\, C_l \\ c\, C_m \\ b\, C_n \end{Bmatrix} \tag{24}$$

The parafoil lift, drag and pitching moment coefficients are nonlinear functions of angle of attack and symmetric brake deflection [5]. Aerodynamic coefficients for the parafoil can be written as [5],

$$C_L = C_L(\alpha_p, \delta_s) + C_{L_{\delta a}}\, \delta_a \tag{25}$$

$$C_D = C_D(\alpha_p, \delta_s) + C_{D_{\delta a}}\, \delta_a \tag{26}$$

$$C_x = C_L \sin\alpha_p - C_D \cos\alpha_p \tag{27}$$

$$C_y = C_{y_{\beta p}}\, \beta_p + C_{y_r} \frac{r_p b}{2 U_p} + C_{y_{\delta a}}\, \delta_a \tag{28}$$

$$C_z = -C_L \cos\alpha_p - C_D \sin\alpha_p \tag{29}$$

$$C_l = C_{l_{\beta p}}\, \beta_p + C_{l_p} \frac{p_p b}{2 U_p} + C_{l_r} \frac{r_p b}{2 U_p} + C_{l_{\delta a}}\, \delta_a \tag{30}$$

$$C_m = C_{m_{ac}}(\alpha_p, \delta_s) + C_{m_q} \frac{q_p c}{2 U_p} + C_{m_{\delta a}}\, \delta_a \tag{31}$$

$$C_n = C_{n_{\beta p}}\, \beta_p + C_{n_p} \frac{p_p b}{2 U_p} + C_{n_r} \frac{r_p b}{2 U_p} + C_{n_{\delta a}}\, \delta_a \tag{32}$$

where, $C_L(\alpha_p, \delta_s)$, $C_D(\alpha_p, \delta_s)$ and $C_{m_{ac}}(\alpha_p, \delta_s)$ are parafoil lift, drag and pitching moment coefficients respectively for a given angle of attack and symmetric brake deflection at zero asymmetric brake deflection.

State Equation

The state equation of the parafoil-payload system using dynamic and kinematic equations from Eqs.(8), (17) and (18) and can be rewritten as,

$$\mathbf{A}\,\dot{\mathbf{X}} = \mathbf{b} \tag{33}$$

or,

$$\dot{\mathbf{X}} = \mathbf{A}^{-1}\,\mathbf{b} \tag{34}$$

$\mathbf{X} \in \Re^{21\text{x}1}$ refers to the state vector of the system given by,

$$\mathbf{X} = \left\{ \omega_b^T \;\; \omega_p^T \;\; \mathbf{v}_o^T \;\; \bar{\mathbf{F}}_o^T \;\; \Theta_b^T \;\; \Theta_p^T \;\; \mathrm{x}_o^T \right\}^T \tag{35}$$

where,

$$\frac{d}{dt}\bar{\mathbf{F}}_o = \mathbf{F}_o \tag{36}$$

$\mathrm{A} \in \Re^{21\text{x}21}$ and $\mathbf{b} \in \Re^{21\text{x}1}$ can be written as,

$$\mathrm{A} = \begin{bmatrix} -m_b[r_{ob}]^{\times} & 0 \in \Re^{3\times3} & m_b T_b & T_b & \\ 0 \in \Re^{3\times3} & -(M_p + M_a)[r_{op}]^{\times} & (M_p + M_a) T_p & -T_p & 0 \in \Re^{12\times9} \\ I_b & 0 \in \Re^{3\times3} & 0 \in \Re^{3\times3} & -[r_{ob}]^{\times} T_b & \\ 0 \in \Re^{3\times3} & I_p & 0 \in \Re^{3\times3} & [r_{op}]^{\times} T_p & \\ 0 \in \Re^{9\times3} & 0 \in \Re^{9\times3} & 0 \in \Re^{9\times3} & 0 \in \Re^{9\times3} & I \in \Re^{9\times9} \end{bmatrix} \tag{37}$$

$$\mathrm{b} = \left\{ \mathrm{b}_1^{\mathrm{T}} \;\; \mathrm{b}_2^{\mathrm{T}} \;\; \mathrm{b}_3^{\mathrm{T}} \;\; \mathrm{b}_4^{\mathrm{T}} \;\; \mathrm{b}_5^{\mathrm{T}} \;\; \mathrm{b}_6^{\mathrm{T}} \;\; \mathrm{b}_7^{\mathrm{T}} \right\}^{\mathrm{T}} \tag{38}$$

where, $\mathbf{b}_5 = \mathbf{C}_b\omega_b$; $\mathbf{b}_6 = \mathbf{C}_p\omega_p$; $\mathbf{b}_7 = \mathbf{v}_o$

Adaptive Controller

In this section, a dynamic adaptive controller similar to Slotine and Li [10] is derived in order to control the parafoil-payload system. Consider a scalar variable s which gives a measure of the error in state of the system, such that,

$$s = \lambda(\tilde{u}_o + \tilde{v}_o + \tilde{w}_o) + \gamma(\tilde{p}_p + \tilde{r}_p) + \eta(\tilde{p}_b + \tilde{r}_b) \quad (39)$$

where, λ, γ and η are strictly positive constant. $\tilde{\mathbf{v}}_o = \{\tilde{u}_o, \tilde{v}_o, \tilde{w}_o\}^T$, $\overline{\omega}_b = \{\tilde{p}_b, \tilde{q}_b, \tilde{r}_b\}^T$ and $\overline{\omega}_p = \{\tilde{p}_p, \tilde{q}_p, \tilde{r}_p\}^T$ are the perturbed system velocity, payload angular velocity and parafoil angular velocity respectively with respect to the trim condition defined as,

$$\tilde{\mathbf{v}}_o = \mathbf{v}_o - \mathbf{v}_{o_{trim}} \quad (40)$$

$$\tilde{\omega}_i = \omega_i - \omega_{i_{trim}} \quad (41)$$

Let $\mathbf{a} \in \Re^{6x1}$ denotes the unknown dynamic coefficient vector,

$$\mathbf{a} = \left\{ C_{l_p} \quad C_{n_p} \quad C_{m_q} \quad C_{y_r} \quad C_{l_r} \quad C_{n_r} \right\}^T \quad (42)$$

If $\hat{\mathbf{a}}$ denotes the estimate of the unknown parameter, the error in the estimate of the unknown parameter can be written as,

$$\tilde{\mathbf{a}} = \hat{\mathbf{a}} - \mathrm{a} \quad (43)$$

Choosing a quadratic Lyapunov function as follows,

$$V(s, \tilde{\mathbf{a}}) = \frac{1}{2}s^2 + \frac{1}{2}\tilde{\mathbf{a}}^T\tilde{\mathbf{a}} \quad (44)$$

It can be seen from Eq.(44) that the chosen positive definite function, V is continuous and differentiable for all $s \in \Re$ and $\tilde{\mathbf{a}} \in \Re^{6x1}$. The time derivative of Lyapunov function can be written as,

$$\dot{V}(s, \tilde{\mathbf{a}}) = s\dot{s} + \dot{\tilde{\mathrm{a}}}^T\tilde{\mathbf{a}} \quad (45)$$

The first term on the right hand side of Eq.(45) can be simplified using Eq.(34) as follows,

$$s\dot{s} = s(\lambda(\dot{u}_o + \dot{v}_o + \dot{w}_o) + \gamma(\dot{p}_p + \dot{r}_p) + \eta(\dot{p}_b + \dot{r}_b)) = s\,\overline{\mathbf{A}}\,\mathbf{b} \quad (46)$$

where, $\overline{\mathbf{A}} \in \Re^{1x21}$ can be written as,

$$\overline{\mathbf{A}} = \lambda\sum_{j=7}^{9}\left[\mathbf{A}^{-1}\right]_j + \gamma\sum_{j=4,6}\left[\mathbf{A}^{-1}\right]_j + \eta\sum_{j=1,3}\left[\mathbf{A}^{-1}\right]_j \quad (47)$$

$[\mathbf{A}^{-1}]_j$ denotes the j^{th} row of the matrix $\mathbf{A}^{-1}$. The vector $\mathbf{b}$ can be broken down into terms containing aerodynamic forces and moments acting on the parafoil and another vector $\overline{\mathbf{b}} \in \Re^{21x1}$ as follows,

$$\mathbf{b} = \overline{\mathbf{b}} + \begin{Bmatrix} 0 \in \Re^{3\times1} \\ \mathbf{F}_{pA} \\ 0 \in \Re^{3\times1} \\ \mathbf{M}_{pA} \\ 0 \in \Re^{9\times1} \end{Bmatrix} \quad (48)$$

Therefore from Eq.(46), it follows that,

$$s\dot{s} = s\left(\overline{\mathbf{A}}\,\overline{\mathbf{b}} + \overline{\overline{\mathbf{A}}}\begin{Bmatrix}\mathbf{F}_{pa}\\ \mathbf{M}_{pa}\end{Bmatrix}\right) \quad (49)$$

where,

$$\overline{\overline{\mathbf{A}}} = \left[\,[\overline{\mathbf{A}}]_4 \;\; [\overline{\mathbf{A}}]_5 \;\; [\overline{\mathbf{A}}]_6 \;\; [\overline{\mathbf{A}}]_{10} \;\; [\overline{\mathbf{A}}]_{11} \;\; [\overline{\mathbf{A}}]_{12}\right] \in \Re^{1x6}.$$

Substituting aerodynamic forces and moments on the parafoil from Eqs.(23) and (24),

$$\overline{\overline{\mathbf{A}}}\begin{Bmatrix}\mathbf{F}_{pa}\\ \mathbf{M}_{pa}\end{Bmatrix} = \frac{1}{2}\rho U_p^2 S_p \overline{\overline{\mathbf{A}}}\begin{Bmatrix} C_x \\ C_y \\ C_z \\ b\,C_l \\ c\,C_m \\ b\,C_n \end{Bmatrix} = H_{\delta a}\delta_a + H_{\beta p}\beta_p + H_o + \mathbf{h}^T\mathbf{a} \quad (50)$$

where,

$$H_{\delta a} = \frac{1}{2}\rho\, v_p^2\, S_p\, \bar{\bar{\mathbf{A}}} \begin{Bmatrix} C_{L_{\delta a}} \frac{w_p}{U_p} - C_{D_{\delta a}} \frac{u_p}{U_p} \\ C_{y_{\delta a}} \\ -C_{L_{\delta a}} \frac{u_p}{U_p} - C_{D_{\delta a}} \frac{w_p}{U_p} \\ bC_{l_{\delta a}} \\ cC_{m_{\delta a}} \\ bC_{n_{\delta a}} \end{Bmatrix} \tag{51}$$

$$H_{\beta p} = \frac{1}{2}\rho\, U_p^2\, S_p\, \bar{\bar{\mathbf{A}}} \begin{Bmatrix} 0 \\ C_{y_{\beta p}} \\ 0 \\ bC_{l_{\beta p}} \\ 0 \\ bC_{n_{\beta p}} \end{Bmatrix} \tag{52}$$

$$H_o = \frac{1}{2}\rho\, U_p^2\, S_p\, \bar{\bar{\mathbf{A}}} \begin{Bmatrix} C_L(\alpha_p, \delta_s) \frac{w_p}{U_p} - C_D(\alpha_p, \delta_s) \frac{u_p}{U_p} \\ 0 \\ -C_L(\alpha_p, \delta_s) \frac{u_p}{U_p} - C_D(\alpha_p, \delta_s) \frac{w_p}{U_p} \\ 0 \\ cC_{m_{ac}}(\alpha_p, \delta_s) \\ 0 \end{Bmatrix} \tag{53}$$

$$\mathbf{h}^T = \frac{1}{2}\rho\, U_p^2\, S_p\, \bar{\bar{\mathbf{A}}} \begin{bmatrix} 0 & 0 & 0 & 0 & 0 & 0 \\ 0 & 0 & 0 & \frac{r_p b}{2U_p} & 0 & 0 \\ 0 & 0 & 0 & 0 & 0 & 0 \\ \frac{p_p b^2}{2U_p} & 0 & 0 & 0 & \frac{r_p b^2}{2U_p} & 0 \\ 0 & 0 & \frac{q_p c^2}{2U_p} & 0 & 0 & 0 \\ 0 & \frac{p_p b^2}{2U_p} & 0 & 0 & 0 & \frac{r_p b^2}{2U_p} \end{bmatrix} \tag{54}$$

Substituting $s\,\dot{s}$ in time derivative of Lyapunov function given in Eq.(45),

$$\dot{V}(s, \tilde{\mathbf{a}}) = s\,(\bar{\mathbf{A}}\,\bar{\mathbf{b}} + H_{\delta a}\,\delta_a + H_{\beta p}\,\beta_p + H_o + \mathbf{h}^T\,\mathbf{a}) + \dot{\tilde{\mathbf{a}}}^T\,\tilde{\mathbf{a}} \tag{55}$$

Control Law

Choosing a control law for the system,

$$\delta_a = \frac{1}{H_{\delta_a}}\,(-\bar{\mathbf{A}}\,\bar{\mathbf{b}} - H_{\beta p}\,\beta_p - H_o - \mathbf{h}^T\,\hat{\mathbf{a}} - K_s\, s) \tag{56}$$

where, K_s is a strictly positive number and $H_{\delta_a} \neq 0$. The chosen control law is substituted in the time derivative of Lyapunov function to obtain the following,

$$\dot{V}(s, \tilde{\mathbf{a}}) = -K_s\, s^2 - s\,\mathbf{h}^T\,\tilde{\mathbf{a}} + \dot{\tilde{\mathbf{a}}}^T\,\tilde{\mathbf{a}} \tag{57}$$

Adaptation Law

The above expression for $\dot{V}$ suggests that we take an adaptation law of the following form,

$$\dot{\tilde{\mathbf{a}}} = s\,\mathbf{h} \tag{58}$$

The adaptation law when substituted in the time derivative Lyapunov function yields,

$$\dot{V}(s, \tilde{\mathbf{a}}) = -K_s\, s^2 \leq 0 \tag{59}$$

It can be seen from Eq.(59) that the time derivative of Lyapunov function is negative definite. Also, the condition of radial unboundedness, $V(s, \tilde{\mathbf{a}}) \rightarrow \infty$ as $|(s, \tilde{\mathbf{a}})| \rightarrow \infty$ is satisfied. Hence, from the Lyapunov theorem of global stability, the chosen control law is globally asymptotically stable. Since the unknown parameter vector **a** is constant, the adaptation law can be alternatively written as,

$$\dot{\hat{\mathbf{a}}} = s\,\mathbf{h} \tag{60}$$

The dependence of control input on estimated parameter vector, $\hat{\mathbf{a}}$ allows it to be a part of the state vector of the system. Therefore, the order of the system increases from 18 to 24 as,

$$\mathbf{X} = \{p_b, q_b, r_b, p_p, q_p, r_p, u_o, v_o, w_o, \phi_b, \theta_b, \psi_b, \phi_p, \theta_p, \psi_p,$$
$$\{x_o, y_o, z_o, \hat{C}_{lp}, \hat{C}_{np}, \hat{C}_{mq}, \hat{C}_{yr}, \hat{C}_{lr}, \hat{C}_{nr}, \}^T$$

Actuator Model

The generation of parafoil trailing edge deflection according to the control law provided in Eq.(56) requires a servo actuator of appropriate control system and bandwidth. A typical servo actuator input can be modelled as a PD (proportional & derivative) system of the angular deflection, given by,

$$u_{act}(t) = K_D \dot{\delta}_a(t) + K_P \delta_a(t) \tag{61}$$

where, K_P and K_D are proportional and derivative gains respectively. If the desirable angular deflection as a function of time is given by Eq.(56), it is clear from Eq.(61) that we have a tracking control problem in hand. We can write Eq.(61) in terms of tracking error, as follows,

$$u_{act}(t) = K_D \dot{e}_{\delta_a}(t) + K_P e_{\delta_a}(t) + K_D \dot{\delta}_{a_d}(t) + K_P \delta_{a_d}(t) \tag{62}$$

A combination of feedback and feedforward control loops for the actuator input leads to the choice of following actuator control law,

$$u_{act}(t) = K_D \dot{\delta}_{a_d}(t) + K_P \delta_{a_d}(t) - K_e e_{\delta_a}(t) \tag{63}$$

where, K_e is a constant feedback gain. It can be noticed that choice of an actuator control law of the form given by Eq.(63) essentially reduces Eq.(62) to a first order linear plant in terms of tracking error as state variable.

Results and Discussions

The simulation is carried out with the system specifications and aerodynamic coefficients given in Tables-1 and 2 respectively, taken from Prakash and Ananthkrishnan [5]. A nonlinear variation of the lift, drag and quarter chord pitching moment coefficients for the parafoil-payload system configuration of Prakash and Ananthkrishnan [5] is shown in Fig.2. The three curves for each of the longitudinal aerodynamic coefficient corresponds to zero symmetric brake deflection ($\delta_s = 0^o$), half symmetric brake deflection ($\delta_s = 45^o$) and full symmetric brake deflection ($\delta_s = 90^o$). The moment transfer in yaw direction at the joint point is assumed to be taking place through a spring-damper of damping coefficient, $c_o = 50$ and stiff-

Table-1 : Parafoil-Payload System Specifications

Parafoil Specifications	
m_p	5 kg
$\boldsymbol{I}_p + \boldsymbol{I}_F$	diag $\begin{pmatrix} 373.87 \\ 127.84 \\ 70.0 \end{pmatrix}$ kgm^2
AR	20
S_p	28 m^2
c	3.75 m
b	7.5 m
t	0.675 m
δ_s	30°
Load Specifications	
m_b	135 kg
$\boldsymbol{I}_b$	diag $\begin{pmatrix} 29.67 \\ 26.76 \\ 42.32 \end{pmatrix}$ kgm^2
S_b	0.5 m^2
C_{D_b}	1.05
Link Specifications	
μ	9°
R_{op}	10 m
R_{ob}	0.5 m
k_o	0
c_o	50

Table-2 : Aerodynamic Coefficients Used in the Simulation

Static Coefficients (known)		Dynamic Coefficients (unknown)	
$C_{y\beta_p}$	- 0.5443	C_{l_p}	- 0.1330
$C_{l\beta_p}$	- 0.0802	C_{n_p}	- 0.0130
$C_{n\beta_p}$	0.0286	C_{m_q}	- 1.864
$C_{L\delta_a}$	0.235	C_{y_r}	- 0.0060
$C_{D\delta_a}$	0.0957	C_{l_r}	0.0100
$C_{y\delta_a}$	0.1368	C_{n_r}	- 0.0350
$C_{l\delta_a}$	- 0.0063		
$C_{m\delta_a}$	0.294		
$C_{n\delta_a}$	0.0155		

ness, $k_o = 0$ so as to absorb the relative vibration between the two subsystems.

The rigging angle, μ is taken to be 9°, as suggested by Machin et al. [3] and later proposed by Prakash and Ananthkrishnan as the optimal rigging angle for good glide and flare characteristics for the current parafoil-payload configuration. A constant symmetric brake deflection, δ_s = 30° is assumed throughout the controller operational time of 100 s. Longitudinal aerodynamic coefficients are found as a function of parafoil angle of attack for the assumed symmetric brake deflection by linear interpolation of the three curves.

The trim and initial conditions for the simulation are shown in Table-3. The small perturbations in the system are assumed by taking initial conditions close to the trim conditions. A generalized case is taken when there is absolutely no knowledge of dynamic coefficients of the parafoil, hence $\hat{a}$ (0) = $\{0, 0, 0, 0, 0, 0\}^T$. The chosen controller parameters are shown in Table-4. The controller parameters however not optimal provide a decent regulation profile to the system.

Simulation results are shown in Figs.3-5. It can be observed in Fig.3 that the settling time of the angular deflections of the system is about 40 s. The system attitude is shown to be settling at the trim value in Fig.5. Fig.6 shows the time history of parafoil angle of attack and sideslip angle. The steady state value of the angle of attack and the sideslip angle is about 58.7° and 5.08° respectively, with a peak value of about 60.16° and 7.02° respectively.

Table-3 : Trim Conditions and Initial Conditions

Trim Conditions		Initial Conditions	
$u_{o_{trim}}$	4.70 m/s	u_o (0)	4.70 m/s
$v_{o_{trim}}$	0.83 m/s	v_o (0)	0.83 m/s
$w_{o_{trim}}$	7.75 m/s	w_o (0)	7.75 m/s
$p_{b_{trim}}$	0 deg/s	p_b (0)	0 deg/s
$q_{b_{trim}}$	0 deg/s	q_b (0)	0 deg/s
$r_{b_{trim}}$	0 deg/s	r_b (0)	0 deg/s
$p_{p_{trim}}$	0 deg/s	p_p (0)	0 deg/s
$q_{p_{trim}}$	0 deg/s	q_p (0)	0 deg/s
$r_{p_{trim}}$	0 deg/s	r_p (0)	0 deg/s
$\phi_{b_{trim}}$	0°	ϕ_b (0)	1°
$\theta_{b_{trim}}$	- 0.62°	θ_b (0)	- 0.62°
$\psi_{b_{trim}}$	10.9°	ψ_b (0)	12.9°
$\phi_{p_{trim}}$	0°	ϕ_p (0)	3°
$\theta_{p_{trim}}$	- 34.26°	θ_p (0)	- 34.26°
$\psi_{p_{trim}}$	10°	ψ_p (0)	11°
		F_{ox} (0)	- 1.035 x 10^4
		F_{oy} (0)	0
		F_{oz} (0)	- 1.114 x 10^5
		$\hat{a}$ (0)	$\{0, 0, 0, 0, 0, 0\}^T$

Table-4 : Chosen Control Parameters

Control Parameters	
λ	15
γ	1500
η	45
K_s	200

The asymmetric brake deflection is shown in Fig.7(a), reaches a steady state value of 0° as desired, in about 40 s. Maximum asymmetric deflection is found to be about -10.54°. It can be observed in Figs.1-7 that the state

variables as well as control input has an oscillatory time profile before system reaches the steady state. Although such oscillatory time profiles generally increases the settling time, on the other hand causes low energy dissipation in the system.

Figure 8 shows the frequency response of the asymmetric deflection angle and actuator input, found by Discrete-Fourier-Transform of the time signal given in Fig.7. A dominant frequency of 0.8 Hz is observed along with two other frequencies of 0.05 Hz and 1.625 Hz. The actuator input frequency response sets a minimum limitation on the choice of actuator control system hardware. In a practical sense, the required bandwidth of the actuator should be at least ten folds of the desired actuator frequency. Based on the frequency content of actuator input shown in Fig.8(b), it can be stated that the minimum actuator bandwidth requirement is relatively smaller and hence easier to implement.

It is evident from the system trajectory as shown in Fig.9 that it follows roughly a straight line path to the ground. Further, the time profiles of joint force and yaw moment are also plotted as shown in Fig.10.

The Lyapunov global stability theorem guarantees the global asymptotic stability of the system with respect to the lateral disturbances. Note that the current method may not necessarily estimate the unknown parameters, but allows the error in state variables to converge to zero [10].

Conclusions

A Lyapunov based dynamic adaptive controller is derived to handle the lateral disturbances in a 9 degree of freedom parafoil-payload system with unknown dynamic coefficients. The current approach closely resembles to the flight control using nonlinear dynamic inversion (NDI). However, the latter requires the knowledge of system parameters, whereas the current approach has an advantage of assuming a dynamic variable as a candidate for the unknown system parameter. Hence, the dynamic variable acts as a state variable which brings the system to its desired state. In addition to this, the Lyapunov based controller also guarantees global asymptotic stability of the system. A 7.5 m span parafoil-payload system under lateral disturbances is numerically shown to stabilize using the present adaptive controller. A relatively smaller control input frequency observed during the simulation will help in easier installation of the control actuator on the system. The current simulation is carried out with typical values of system parameters and initial conditions giving a satisfactory time as well as frequency response. However, in a situation of severe gusts the robustness of the present control law is still needed to be checked.

Acknowledgements

The authors are grateful to Aerial Delivery Research and Development Establishment, Agra for their support.

References

1. Nicolaides, J. D., "Flight Test Results of a Powered Parafoil System", Technical Report AFFDL TR-76-15, pp.31, 1976.

2. Wailes, W. K. and Harrington, N. E., "The Guided Parafoil Airborne Delivery System Program", AIAA Paper 95-1538, May, 1995.

3. Machin, R. A., Iacomini, C. S., Cerimele, C. J. and Stein, J. M., "Flight Testing the Parachute System for the Space Station Crew Return Vehicle", Journal of Aircraft, Vol.38, No.5, pp.786-799, 2001.

4. Slegers, N. and Costello, M., "Aspects of Control for a Parafoil and Payload System", Journal of Guidance, Control, and Dynamics, Vol.26, No.6, pp.898-905, 2003.

5. Prakash, O. and Ananthkrishnan, N., "Modelling and Simulation of 9-DOF Parafoil-payload System Flight Dynamics", Atmospheric Flight Mechanics Conference and Exhibit, AIAA, Colorado, August, 2006.

6. Gorman, C. M. and Slegers, N. J., "Evaluation of Multibody Parafoil Dynamics Using Distributed Miniature Wireless Sensors", Journal of Aircraft, Vol.49, No.2, pp.546-555, 2012.

7. Slegers, N. and Costello, M., "Model Predictive Control of a Parafoil and Payload System", Atmospheric Flight Mechanics Conference and Exhibit, AIAA, Providence, Rhode Island, August, 2004.

8. Slegers, N., Beyer, E. and Costello, M., "Use of Variable Incidence Angle for Glide Slope Control of Autonomous Parafoils", Journal of Guidance, Control, and Dynamics, Vol.31, No.3, pp.585-596, 2008.

9. Lissaman, P. B. S. and Brown, G. J., "Apparent Mass Effects on Parafoil Dynamics", Technical Report 93-1236, American Institute of Aeronautics and Astronautics, 1993.

10. Slotine, J. J. E. and Li, W., "On the Adaptive Control of Robot Manipulators", The International Journal of Robotics Research, Vol. 6, No. 3, pp. 49-59, 1987.

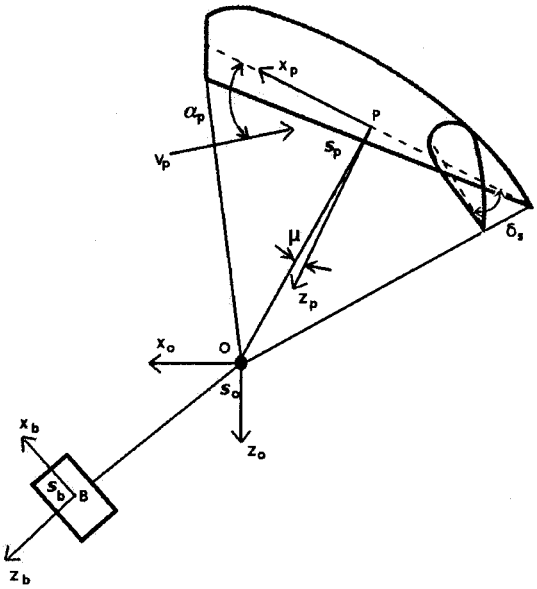

Fig.1 A Parafoil-Payload System

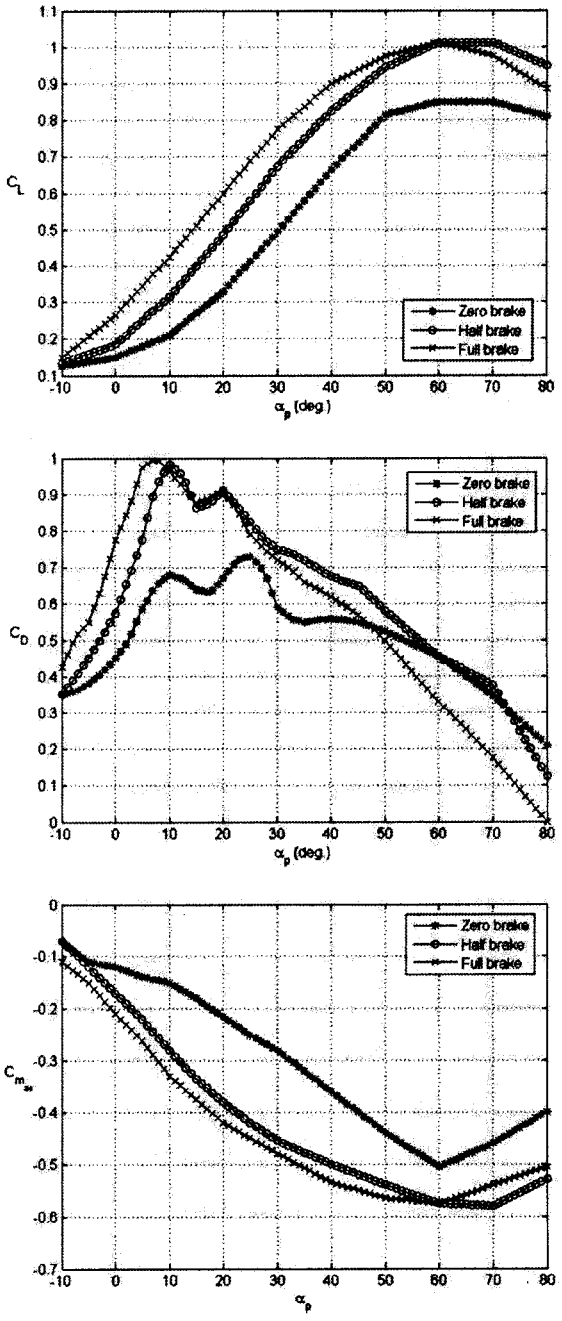

Fig.2 Longitudinal Aerodynamic Data

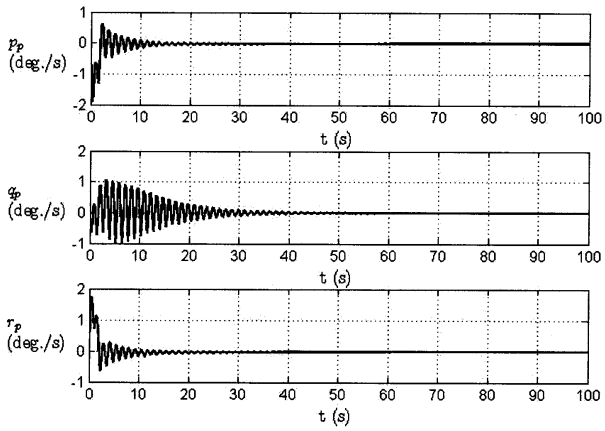

Fig.3a Parafoil Angular Rate

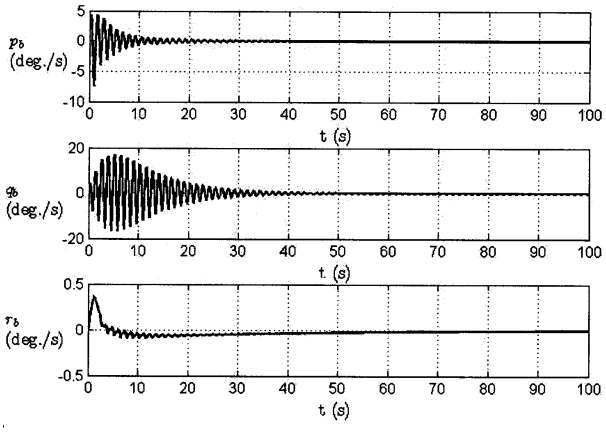

Fig.3b Payload Angular Rate

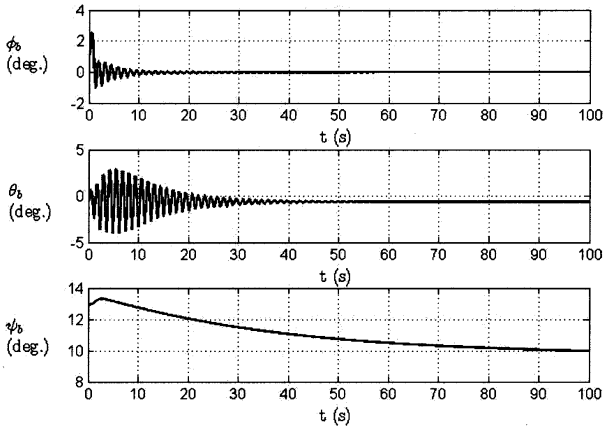

Fig.5b Payload Attitude

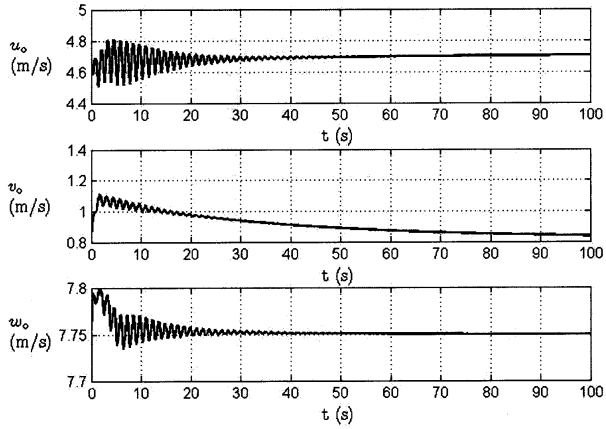

Fig.4 System Velocity (or Joint Point Velocity)

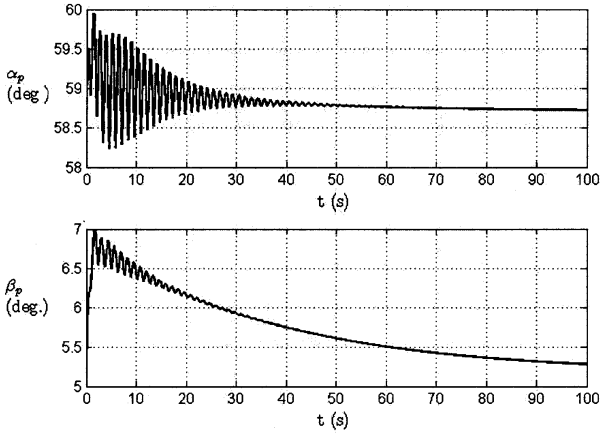

Fig.6 Parafoil Angle of Attack and Sideslip Angle

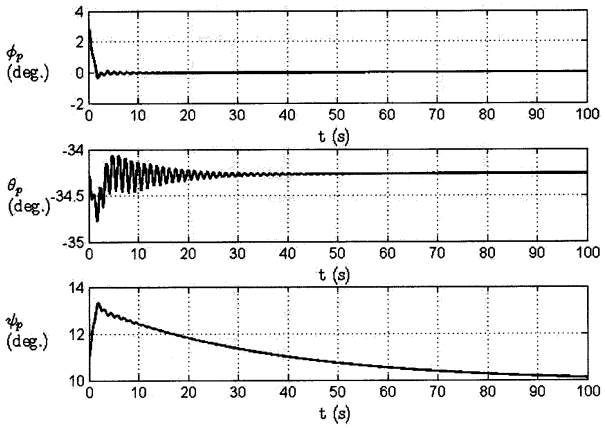

Fig.5a Parafoil Attitude

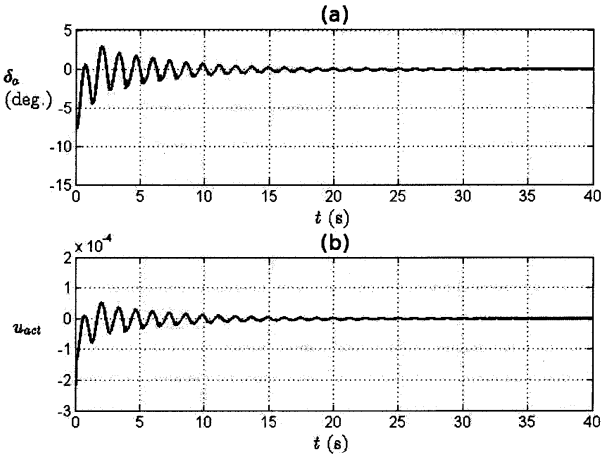

Fig.7 (a) Asymmetric Brake Deflection and (b) Actuator Input

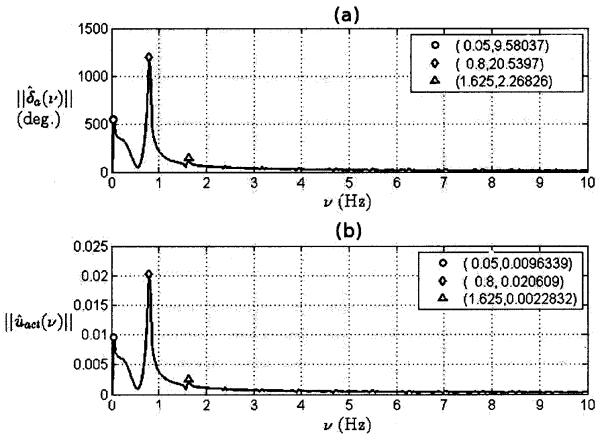

Fig.8 Frequency Response of (a) Asymmetric Brake Deflection and (b) Actuator Input

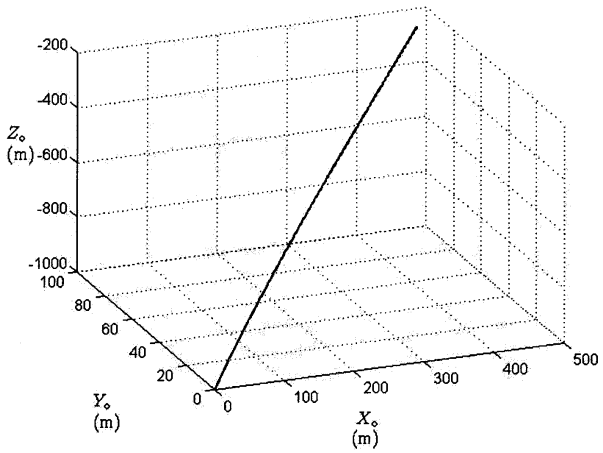

Fig.9 Trajectory

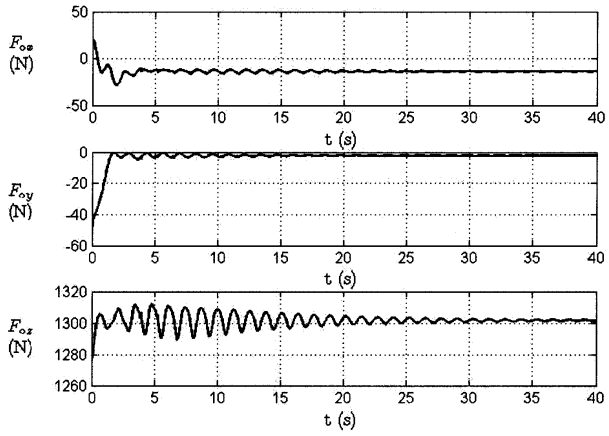

Fig.10a Joint Force

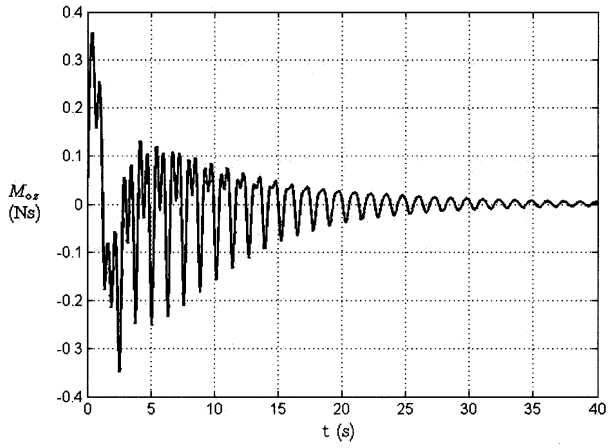

Fig.10b Joint Moment